AIP | The Journal of Chemical Physics

# Charge transport in organic crystals: Critical role of correlated fluctuations unveiled by analysis of Feynman diagrams

Daniel M. Packwood, Kazuaki Oniwa, Tienan Jin, and Naoki Asao

Citation: The Journal of Chemical Physics **142**, 144503 (2015); doi: 10.1063/1.4916385
View online: http://dx.doi.org/10.1063/1.4916385
View Table of Contents: http://scitation.aip.org/content/aip/journal/jcp/142/14?ver=pdfcov
Published by the AIP Publishing



# Charge transport in organic crystals: Critical role of correlated fluctuations unveiled by analysis of Feynman diagrams

Daniel M. Packwood, Kazuaki Oniwa, Tienan Jin, and Naoki Asao
*Advanced Institute for Materials Research, Tohoku University, Sendai, Japan*

(Received 23 October 2014; accepted 18 March 2015; published online 9 April 2015)

Organic crystals have unique charge transport properties that lie somewhere between delocalised band-type transport and localised hopping transport. In this paper, we use a stochastic tight-binding model to explore how dynamical disorder in organic crystals affects charge transport. By analysing the model in terms of Feynman diagrams (virtual processes), we expose the crucial role of correlated dynamical disorder to the charge transport dynamics in the model at short times in the order of a few hundred femtoseconds. Under correlated dynamical disorder, the random motions of molecules in the crystal allow for low-energy "bonding"-type interactions between neighboring molecular orbitals can persist over long periods of time. On the other hand, the dependence of charge transport on correlated dynamical disorder also tends to localize the charge, as correlated disorder cannot persist far in space. This concept of correlation may be the "missing link" for describing the intermediate regime between band transport and hopping transport that occurs in organic crystals. © *2015 AIP Publishing LLC.* [http://dx.doi.org/10.1063/1.4916385]

## I. INTRODUCTION

Despite decades of intensive research, the nature of charge transport in high mobility organic crystals such as rubrene or pentacene remains controversial. In general, charge transport in organic crystals is characterised by two properties that are difficult to explain with conventional charge transport models,[1] namely, that near room temperature (a) electron and hole mobilities decrease in a power-law fashion with temperature[2] and (b) the mean free paths of electrons and holes are comparable to the crystal's unit cell size.[3] Property (a) is suggestive of delocalised band-type transport, with scattering by thermal molecular motions at higher temperature, whereas property (b) is suggestive of highly localised hopping transport between unit cells. Moreover, in the usual hopping transport picture, transport is activated by temperature. In order to reconcile these properties, simplified models with broad generality and mathematical analysis are extremely useful.

A long-established approach for studying temperature dependence of mobility in crystals is via polaron trapping of electrons (i.e., "local" electron-phonon interactions).[4] An important prediction of such theories is a crossover from band-type transport to hopping-type transport as temperature increases. For organic crystals, these theories explain property (b) well, however, they often run into difficulties in explaining (a). In more recent years, attention has turned to the large presence of *dynamical disorder* in organic crystals. This dynamical disorder, which arises from the erratic thermal motion of the molecules (inter-molecular phonon modes), is particularly conspicuous in organic crystals because the relatively weak van der Waals bonding between molecules allows for a large amount of molecular motion at room temperature.[5] The effect of dynamical disorder has been explored in recent years with a variety of theoretical approaches, including generalisations of the Holstein-Peierls model,[6–10] the hierarchy equations of motion,[11] and mixed quantum-classical models based on molecular dynamics or stochastic models of the molecular framework.[12–15] First principles calculations and molecular dynamics simulations have shown that the thermal molecular motions cause large modulation of the electronic coupling between molecules (i.e., "non-local electron-phonon" coupling) and dynamical localisation of charges,[12,16] This large modulation of the electronic coupling is due to the relatively large distances between adjacent molecules in the crystal and the complicated shape of the frontier orbitals of each molecule; small thermal motions of the molecules tend to produce erratic changes in both the sign and magnitude of the coupling.[17,18] This modulation could be considered as stochastic. At present, there appears to be a consensus in the literature that dynamical disorder and electron-phonon coupling are the central phenomena behind the charge transport properties (a) and (b). However, the unifying concept that underlies the calculation output and *connects* the dynamical disorder to charge transport mechanism in organic crystals has still not been highlighted.

In this paper, we study a tight-binding model with stochastic site-site coupling ("stochastic tight binding model"). This model is distinct from the widely studied Gaussian disorder models, which consider stochastic site energies.[19,20] While stochastic models can be used to model experimental data, they are especially convenient for exploring how intuitive concepts such as "correlation" and "amplitude" of the stochastic noise contribute to the model output. This latter quality of the stochastic models is of particular interest to the present paper. By a mathematical analysis of the stochastic tight-binding (STB) model, we identify a key set of Feynman diagrams that describe the charge transport physics. These Feynman diagrams highlight the central role of *correlated stochastic modulation* in the charge transport mechanism in the STB model. Correlated stochastic modulation means that under dynamical disorder, the relative orientation between molecular

 

orbitals in the crystal remains relatively stable over time and over short distances. This then means that "bonding"-type interactions between neighboring molecular orbitals can survive on time scales comparable to charge transport between the molecules. On the other hand, uncorrelated stochastic modulation means that the relative orientation of molecular orbitals changes erratically under the dynamical disorder, which rapidly destroys bonding-type interactions and impedes charge transport. We will propose that this "correlated dynamical disorder-dependent" charge transport mechanism leads to a consistent explanation of properties (a) and (b) in organic crystals.

This paper is organized as follows. Sec. II describes the model and presents a simulation. Sec. III describes the analysis and presents the key results. Sec. IV contains a discussion and conclusions.

## II. STOCHASTIC TIGHT-BINDING MODEL

The STB model Hamiltonian considers a single electron spreading over a collection of molecular orbitals located at the sites $V$ of a lattice $G$, namely,

$$\hat{H}(t) = \sum_{v \in V} \varepsilon_v |v\rangle \langle v| + \sum_{(u,v) \in E} T_{uv}(t) |u\rangle \langle v| . \quad (1)$$

In Eq. (1), $|v\rangle$ is the state of the electron when localised to the molecular orbital (LUMO) at $v$, $\varepsilon_v$ is the energy of state $|v\rangle$, $E$ is all pairs of nearest neighbors in $G$, and $T_{uv}(t)$ is the transfer integral between orbitals at sites $u$ and $v$. For each pair of nearest neighbors $uv$, $T_{uv}(t)$ is assumed to be of the form,

$$T_{uv}(t) = w_{uv} + X_{uv}(t), \quad (2)$$

where $w_{uv}$ is a time-independent term and $X_{uv}(t)$ is a Gaussian stochastic process. This Gaussian process describes stochastic modulation of the electronic coupling between molecules due to dynamical disorder in the crystal. Similar models have been proposed by other authors and have successfully captured the qualitative (and sometimes quantitative) properties of charge transport in organic crystals near room temperature.[12,15,16,21] We suppose that $E[X_{uv}(t)] = 0$ for all times and every pair of neighboring orbitals in the lattice, where $E$ denotes an ensemble average (statistical expected value), and that $X_{uv}(t)$ is stationary and Markov. By "ensemble," we mean infinite and independent copies of the lattice $G$, each with a single electron and independent Gaussian modulations. Due to these properties, we have that the correlation functions of $X_{uv}(t)$ decay exponentially with time.[22] For any two pairs of nearest neighbors $uv$ and $rw$, we therefore set

$$E[X_{uv}(t) X_{rw}(s)] = \begin{cases} 2\sigma^2 e^{-c(t-s)}, & uv = rw \\ \sigma^2 e^{-c(t-s)}, & uv \sim rw \\ 0, & \text{otherwise} \end{cases}, \quad (3)$$

for $t \geq s$, where $c$ is the decorrelation rate of the Gaussian modulation and $\sigma^2$ is a constant. $uv = rw$ means that the two pairs of nearest neighbors are identical and $uv \sim rw$ means that the pairs are adjacent in the lattice (i.e., that one of $u$ or $v$ equals either $r$ or $w$). The assumption that the correlation between adjacent pairs is half the size of the correlation of a single pair is mainly out of convenience; however, partial justification is provided in the Appendix. Under these conditions, $\sigma^2$ in Eq. (3) works out to be $\sigma^2 = b^2/2c$, where $b$ is a constant which measures the amplitude of the stochastic modulation (see the Appendix). Because this stochastic approach does not contain enough detail to describe the temperature of the lattice, we will study the STB model as a function of the decorrelation rate $c$. $c$ is expected to increase as a positive power of temperature. This study is therefore concerned with how the correlation of the stochastic noise affects the electron dynamics in the STB model.

The state of the electron for a particular lattice in the ensemble is described with the wave function $|\psi(t)\rangle = \sum_{v \in V} c_v(t) e^{i\varepsilon t/\hbar} |v\rangle$ and density operator $\rho(t) = |\psi(t)\rangle\langle\psi(t)| = \sum_{u,v} c_u^*(t) c_v(t) |u\rangle\langle v|$. The quantities that are relevant to a real experiment are the ensemble averages of the diagonal elements of $\rho(t)$, i.e.,

$$P_k(t) = E\left[c_k^*(t) c_k(t)\right]. \quad (4)$$

We refer to the $P_k(t)$'s as the "distribution of the electron;" if we generate an electron at site 0 on each lattice in the ensemble, then $P_k(t)$ is the probability that we will find the electron at position $k$ at time $t$ if we randomly choose a lattice from the ensemble and measure the state of its electron. We have calculated the distribution of the electron spreading over a single plane of an anthracene lattice (space group $P2_1/a$), as shown in Figure 1. This was calculated by simulating a trajectory for each of the stochastic processes in (1) using Gillespie's algorithm[23] and solving the Schrodinger equation using the Hamiltonian (1). This was repeated ten times, and the average of the square amplitude of the wave function coefficients was calculated for each time point. Crystal structure data and values for the transfer integrals were taken from Refs. 24 and 16, respectively. Each simulation used 496 anthracene molecules, $c$ was set to 0.005 $\text{fs}^{-1}$, and the constant $b$ was set to 375.7 $\text{cm}^{-1} \times 1\ \text{fs}^{-1}$, where 375.7 $\text{cm}^{-1}$ is the standard deviation of the transfer integrals estimated in Ref. 16 for neighboring molecules of type (A) (see Figure 1(a)). The diagonal elements of the Hamiltonian for neighbors of type (B) were then multiplied by a factor of 496.6 $\text{cm}^{-1}/357.7\ \text{cm}^{-1}$, where 496.6 $\text{cm}^{-1}$ is the standard deviation for transfer integrals for neighbors of type (B) estimated in Ref. 16. These calculations show how the distribution of the electron spreads across the anthracene lattice and does not show any unexpected features. To study the mobility of the electron, we define the *stochastic mobility*,

$$\mu_s = D/c, \quad (5)$$

where $c$ is the decorrelation rate and $D$ is the diffusion coefficient,

$$D = \lim_{t \to \infty} \frac{1}{2t} \sum_{k=-N}^{N} k^2 P_k(t). \quad (6)$$

The stochastic mobility is analogous to Einstein's formula, but with the factor $k_B T$ (Boltzmann constant × temperature) in the denominator replaced with the decorrelation rate. Figure 1(e) plots $\mu_s$ for a variety of decorrelation rates, as estimated from simulations of the type described above. $\mu_s$ decays

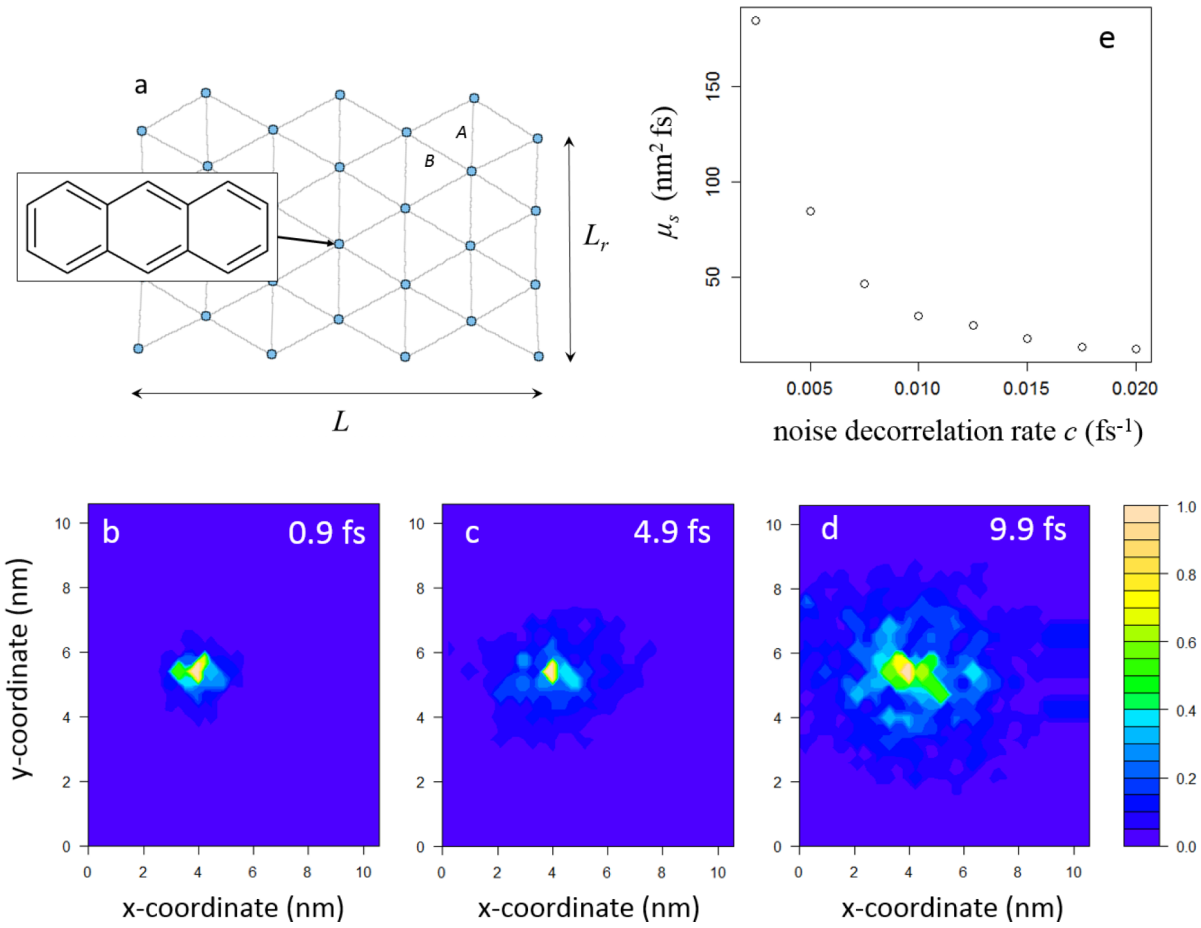


FIG. 1. Simulation of the stochastic tight-binding model for an anthracene crystal. (a) Graph for an anthracene crystal plane. The inset shows an anthracene molecule. The anthracene crystal has two types of edges (labeled A and B), which differ in lengths and the electronic coupling between the molecules. The simulation considered $L_r \times L = 16 \times 31 = 496$ sites, with the electron initially localised to the vertex closest to center of the crystal. Transfer integrals ($-629.6$ cm$^{-1}$ for A edges and 426.7 cm$^{-1}$ for B edges) and standard deviations for the stochastic modulation (375.7 cm$^{-1}$ for A edges and 496.6 cm$^{-1}$ for B edges) were taken from Ref. 16 Crystal structure data (0.604 nm for A edges, 0.470 nm for B edges) were taken from Ref. 24. The anthracene network was produced with the iGraph package for $R$.[37,38] [(b) and (c)]. Plot of the electron distribution $P_k(t)$ for various times. The lack of smoothness is due to the relatively small number of samples used to compute the electron distribution (10 samples in this case). (d) Plot of the stochastic mobility as a function of then noise decorrelation rate.

in a power-law fashion with decorrelation rate. This is qualitatively the same temperature dependence as seen for electron and hole mobilities near room temperature in real experiments on anthracene single crystals.[25,26] Note that the values of the decorrelation rate used here appear to be reasonable because intermolecular motion is expected to take place on a scale of at least 100 fs,[1] which suggests that $c$ should be in the order of around 0.01 fs$^{-1}$. Qualitatively similar results are obtained when using longer simulation times (50 fs) and larger values of $c$ in the order of 1 fs$^{-1}$ (which helps to facilitate long-time calculations).

In addition to the decorrelation rate $c$ in Eq. (3), the amplitude parameter $\sigma$ is also expected to increase in a power-law fashion. The supplementary material presents calculations of the mobility of the electron as a function of the amplitude of the stochastic modulation at fixed decorrelation rate $c$.[40] For this case, we see qualitatively similar behavior to the mobility dependence on decorrelation rate shown in Figure 1. According to the STB model, the decay of electron mobility with temperature in real organic crystals can therefore be attributed to either an increase in the amplitude of the molecular motions in the crystal, an increase in the decorrelation rate of the molecular motions, or both.

## III. ANALYSIS OF VIRTUAL PROCESSES

A mathematical analysis, as opposed to a simulation, is necessary to extract the key physics in the STB model. We will consider the simpler case of a 1D chain containing $L = 2N + 1$ molecules, and for all pairs of neighbors $uv$, we set $w_{uv} = 0$ and assume that the $X_{uv}$ are identically distributed (i.e., have the same moments). The simplication $w_{uv} = 0$ means that electron transport is dominated by thermal fluctuations. As shown in the supplementary material,[40] the stochastic mobility in this model displays similar qualitative dependence on the decorrelation rate $c$ as seen in the anthracene calculations described above. However, an important difference for this case compared to the anthracene case is that increasing the amplitude of the stochastic modulation increases the electron mobility (unless very large amplitude stochastic modulation is used), as might be expected in a regime in which electron transport is dominated by

thermal fluctuations. Strictly speaking, the following analysis is relevant to real organic crystals in which the temperature dependence of the charge transport mechanism is projected mainly through the decorrelation rate parameter rather than the amplitude parameter of the stochastic modulation. On the other hand, the supplementary material also discusses a more general case where $w_{uv} = w$ for each pair of neighbors $uv$, and essentially, the same results are shown to apply (particularly the main results in Eqs. (12) and (14)), so the conclusions that are drawn here are expected to apply for more general cases as well.

In the following, all operators will be considered in the interaction picture, with the time-independent part of the Hamiltonian as $\hat{H}_0 = \sum_{k=-N}^{N} \varepsilon |k\rangle\langle k|$ and time-dependent part as $\hat{W}(t) = \sum_{u\sim v} X_{uv}(t) |u\rangle\langle v|$. We consider the diagonal elements of the time-dependent perturbative expansion of the density matrix,

$$\hat{\rho}_{kk}(t) = \hat{\rho}_{kk}(0) + \sum_{n=1}^{\infty} \left(\frac{-i}{\hbar}\right)^n \int_0^t d\tau_n \int_0^{\tau_n} d\tau_{n-1} \cdots \int_0^{\tau_2} d\tau_1 \times \langle k| \left[\hat{W}(\tau_n), \left[\hat{W}(\tau_{n-1}), \ldots, \left[\hat{W}(\tau_1), \hat{\rho}(0)\right], \ldots\right]\right] |k\rangle, \tag{7}$$

where $\hat{\rho}(0) = |0\rangle\langle 0|$. If we expand the commutators in Eq. (7) and perform the matrix multiplications of the $\hat{W}$ operators, we obtain a number of terms. Each such term can be interpreted as a *virtual process* and can be described with a (double-sided) Feynman diagram.[27] The Feynman diagram describing the term $X_{23}(\tau_6) X_{32}(\tau_5) X_{21}(\tau_4) X_{10}(\tau_2) X_{01}(\tau_1) X_{12}(\tau_3)$ is shown in Figure 2(a). This Feynman diagram describes a virtual process where the ket $|0\rangle$ of the initial density matrix $|0\rangle\langle 0|$ makes transitions to states $|1\rangle$, $|2\rangle$, $|3\rangle$, and then back to $|2\rangle$ at times $\tau_2$, $\tau_4$, $\tau_5$, and $\tau_6$, respectively, and the bra $|0\rangle$ makes transitions to states $|1\rangle$ and then $|2\rangle$ at times $\tau_1$ and $\tau_3$, respectively. The transitions are induced by the Gaussian modulation. The transition times of the ket and bra occur in *increasing order* starting from the initial states.

Figures 2(e) and 2(f) show the *cycles* corresponding to the Feynman diagrams in Figures 2(a)–2(d). The cycle is a graph

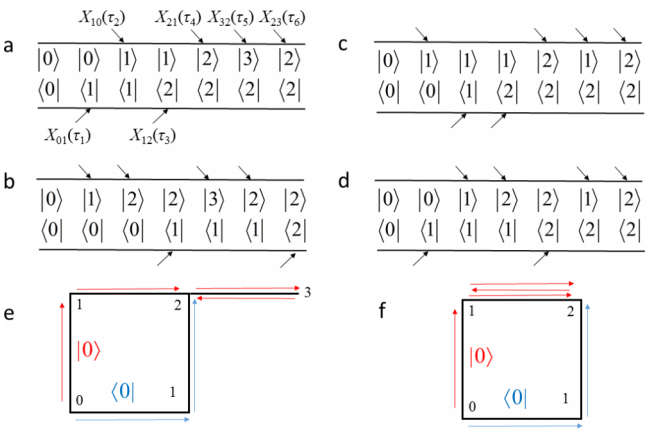


FIG. 2. Feynman diagrams for the terms (a) $X_{23}(\tau_6)X_{32}(\tau_5)X_{21}(\tau_4)X_{10}(\tau_2)X_{01}(\tau_1)X_{12}(\tau_3)$, (b) $X_{23}(\tau_5)X_{32}(\tau_4)X_{21}(\tau_2)X_{10}(\tau_1)X_{01}(\tau_3)X_{12}(\tau_6)$, (c) $X_{21}(\tau_6)X_{12}(\tau_5)X_{21}(\tau_4)X_{10}(\tau_1)X_{01}(\tau_2)X_{12}(\tau_3)$, and (d) $X_{21}(\tau_6)X_{12}(\tau_5)X_{21}(\tau_3)X_{10}(\tau_2)X_{01}(\tau_1)X_{12}(\tau_4)$. (e) The cycle corresponding to the virtual processes in (a) and (b). (f) The cycle corresponding to the virtual processes in (c) and (d).

which shows the transitions of the bra and ket in the virtual process described by the Feynman diagram. A cycle is drawn such that the bra and ket pathways do not overlap, but with the bra and ket, both starting and finishing at the same vertex. The lines connecting the vertices in a cycle are called edges. The arrows show how many times an edge is crossed by the bra or ket, and also the direction in which the edge is crossed. The order of a cycle is the number of edges in the cycle. Because cycles do not contain any time-ordering information, a single cycle may correspond to several Feynman diagrams. This property allows us to classify different kinds of Feynman diagrams according to their cycles. Accordingly, the ensemble average of (7) can be written as

$$P_k(t) = \delta_{0k} + \sum_{n=2,4,6,\ldots}^{\infty} (-i/\hbar)^n \int_0^t d\tau_n \int_0^{\tau_n} d\tau_{n-1} \cdots \int_0^{\tau_2} d\tau_1 \times \sum_{C\in\mathbf{C}_n} \sum_{f\in\mathbf{F}(C)} E\left[f(\tau_1, \ldots, \tau_n)\right], \tag{8}$$

where $\mathbf{C}_n$ is the collection of all cycles of order $n$, $\mathbf{F}(C)$ is the collection of all Feynman diagrams with cycle $C$, and $E[f(\tau_1, \ldots, \tau_n)]$ is the correlation function for the stochastic modulation in the virtual process described the Feynman diagram $f(\tau_1, \ldots, \tau_n)$ (i.e., for the Feynman diagram for the term $X_{21}(\tau_2) X_{10}(\tau_1) X_{01}(\tau_3) X_{12}(\tau_4)$, $E[f(\tau_1,\tau_2,\tau_3,\tau_4)] = E[X_{21}(\tau_2) X_{10}(\tau_1) X_{01}(\tau_3) X_{12}(\tau_4)]$). Only even-order cycles appear in Eq. (8), as odd-order cycles are not possible for a one-dimensional chain. Equation (8) is referred to as the *cycle expansion of the electron distribution*.

We wish to identify the cycles that have virtual processes which make the dominant contributions to Eqs. (7) and (8). Consider the correlation functions $E[f(\tau_1, \ldots, \tau_n)]$ in Eq. (8). In general, $f(\tau_1, \ldots, \tau_n) = X_{e_1}(\tau_1) X_{e_2}(\tau_2) \cdots X_{e_n}(\tau_n)$, where $e_k$ denotes the edge in the cycle that is crossed at time $\tau_k$ due to stochastic modulation. For even $n$, Isserlis's theorem on moments of products of Gaussian random variables[28–30] and Eq. (3) gives

$$E\left[f(\tau_1, \ldots, \tau_n)\right] = \sigma^n (-1)^h \sum_{p\in\pi(C)} \prod_{(e_u,e_v)\in p} \chi(e_u, e_v) \exp\left(-c\,|\tau_u - \tau_v|\right). \tag{9}$$

In Eq. (9), $\pi(C)$ is the collection of all partitions of the edges of $C$ into $|C|/2$ pairs, where $|C| = n$ is the order of $C$, $\chi(e_u, e_v) = 2$ if $e_u = e_v$, $\chi(e_u, e_v) = 1$ if $e_u \sim e_v$, and $\chi(e_u, e_v) = 0$ otherwise (see Figure 3 for an explanation of the notation). The factor $(-1)^h$ arises from the $h$ transitions made by the bra of the density matrix $\langle 0|$ in the virtual process (the –1 factor appears when expanding the commutators in Eq. (7)). Using the same notation as used in Eq. (9), we define the *cycle degeneracy* (Figure 3),

$$\alpha(C) = \sum_{p\in\pi(C)} \prod_{(e_u,e_v)\in p} \chi(e_1, e_2). \tag{10}$$

Degeneracies for a range of cycles are shown in Figure 4. Cycles that involve multiple crossings of the same edges tend to have very large degeneracies. Note that for any Feynman diagram $f$ with cycle $C$ of order $n$, we have that the correlation

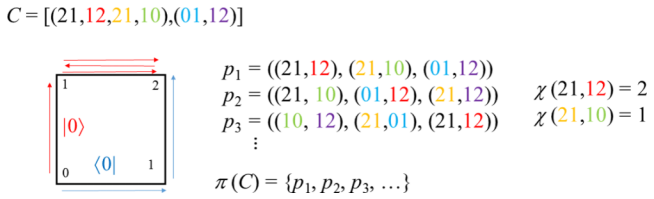


FIG. 3. Illustration of the notation in Eqs. (9) and (15).

function is in the order of magnitude $\sigma^n \alpha(C)$, i.e.,

$$E[f(\tau_1, \ldots, \tau_n)] = O(\sigma^n \alpha(C)). \tag{11}$$

The degeneracy of a cycle $C$ can therefore be used to estimate the correlation of stochastic modulation in any virtual process with cycle $C$. For this reason, we therefore refer to a cycle with large degeneracy as a *correlated cycle*.

In the Appendix, we prove a mathematical theorem that shows that the electron dynamics can be approximated by only considering correlated cycles. More specifically, this theorem says the following. Choose some small positive number $\gamma$. Now, suppose that we can identify a subset $\mathbf{C}_n^{1-\gamma}$ of the cycles in $\mathbf{C}_n$ such that the following holds for each $n$:

$$\frac{\sum_{C \in \mathbf{C}_n^{1-\gamma}} \alpha(C)}{\sum_{C \in \mathbf{C}_n} \alpha(C)} > 1 - \gamma. \tag{12}$$

The inequality in (12) says that the degeneracies of the cycles from $\mathbf{C}_n^{1-\gamma}$ account for over $100(1-\gamma)\%$ to the sum of degeneracies. In other words, the cycles from $\mathbf{C}_n^{1-\gamma}$ are highly correlated cycles. Then, under these conditions, we have (see the Appendix)

$$P_k(t) = P_k^{1-\gamma}(t) + \varepsilon(t), \quad 0 \le |\varepsilon(t)| \le \gamma e^{ct}/(1-\gamma), \tag{13}$$

where $P_k^{1-\gamma}(t)$ is the cycle expansion in (8) but with the cycles in the set $\mathbf{C}_n$ replaced by the smaller set $\mathbf{C}_n^{1-\gamma}$ of correlated cycles. In short, this result says that we can approximate the ensemble-averaged dynamics of the electron at short times by neglecting the contribution of cycles with small correlation, providing that we can identify a $\gamma$ such that (12) holds. From this result, we can also obtain a conclusion for the dynamics of individual electrons in the ensemble, namely, that there exists a number $\gamma_0 < \gamma$ and a superset $\mathbf{C}_n^{1-\gamma_0}$ of $\mathbf{C}_n^{1-\gamma}$ (i.e., $\mathbf{C}_n^{1-\gamma_0}$ contains every cycle of $\mathbf{C}_n^{1-\gamma}$ and as well as some other cycles from $\mathbf{C}_n$) such that

$$\Pr\left(\left|\rho_{kk}(t) - \rho_{kk}^{1-\gamma_0}\right| < \varepsilon e^{ct}\right) = 1, \tag{14}$$

where $\rho_{kk}^{1-\gamma_0}(t)$ is the perturbative expansion in (7) but calculated only with Feynman diagrams with cycles in $\mathbf{C}_n^{1-\gamma_0}$, Pr is a probability, and $\varepsilon$ is a small positive number. Equation (14) says that the deviation of the approximated dynamics $\rho_{kk}^{1-\gamma_0}(t)$ of any individual electron in the ensemble is within $\varepsilon e^{ct}$ of the true dynamics $\rho_{kk}(t)$. A formal statement of these results and a proof are provided in the Appendix. Note that it does not appear to be possible avoid to the factor $e^{ct}$ without introducing significant technical difficulties into the mathematics. The following analysis must be restricted to short times only. For real organic crystals in which $c$ is expected to be in the order of 0.01 fs$^{-1}$, we obtain an upper-bound error $\gamma e^{ct}/(1-\gamma)$ of 2.7% for $t = 100$ fs and of 7.4% for $t = 200$ fs when we set $\gamma = 0.01$. The approximations in Eqs. (13) and (14) are therefore relevant to the early stages of the electron interaction with the intermolecular vibrations of the lattice, which occur on a time scale of at least 100 fs.[1]

In order to verify if the approximations in Eqs. (13) and (14) hold for the STB model, we must identify a set $\mathbf{C}_n^{1-\gamma}$ of correlated cycles that satisfy (12). A reasonable candidate for $\mathbf{C}_n^{1-\gamma}$ is cycles which are highly localised about site 0 in the lattice. The localisation of a cycle can be measured with the *cycle variance*. For a given cycle $C$ containing vertices $v_1, v_2, \ldots, v_m$,[31] the variance of $C$ is defined as

$$s_C^2 = \frac{1}{m} \sum_{k=1}^{m} (v_k - \bar{v}_C)^2, \tag{15}$$

where $\bar{v}_C$ is the *cycle mean*, $\bar{v}_C = (1/m)\sum_{k=1}^{m} v_k$. The cycle variance is shown for various cycles in Figure 4. A small variance means that the cycle is relatively localised across the lattice. Figure 5 shows a calculation of the cycle variance for all cycles with orders $n = 10$, 12, and 14 (the method used for generating the cycles is outlined in the Appendix). Figure 5 is interpreted as follows. Consider a set of cycles,

$$\mathbf{C}_n^q = \{C \in \mathbf{C}_n : s^2(C) > q\}. \tag{16}$$

(This notation is read as "the subset of cycles in $\mathbf{C}_n$ with variance greater than $q$.") The $x$-axis of Figure 5 is in units of $q$, and the $y$-axis of is the contribution of the cycles in $\mathbf{C}_n^q$ to the sum of degeneracies of $\mathbf{C}_n$. The plots show long tails and identify cycles with $s_C^2$ greater than about 1.5 as making a negligible contribution to the sum of the degeneracies. We expect similar results for cycles with lengths greater than 14; however, we were unable to perform this calculation due to hardware limitations. This analysis strongly suggests that we can identify the "important cycles." $\mathbf{C}_n^{1-\gamma}$ in Eq. (12) as the cycles with small variance, i.e.,

$$\mathbf{C}_n^{1-\gamma} = \{C \in \mathbf{C}_n : s_C^2 \le q\}, \tag{17}$$

where $q$ is in the order of about 1.5 and $\gamma$ is in the order of about 0.01. In order to visualise how many cycles from

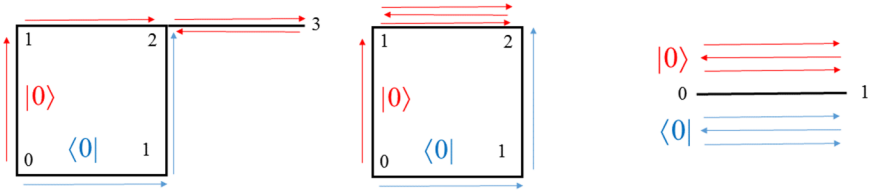


FIG. 4. Degeneracies and variances of some cycles.

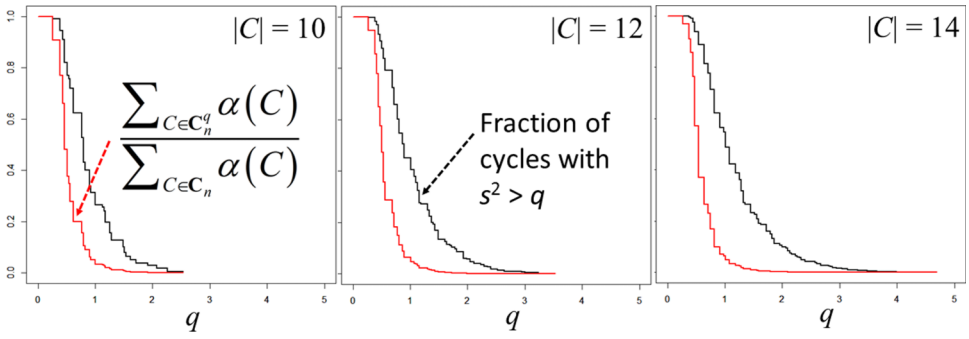


FIG. 5. (Red) Contribution of the subsets of cycles $\mathbf{C}_n^q = \{C \in \mathbf{C}_n : s^2(C) > q\}$ to the sum of degeneracies for cycles with length $n = 10$, 12, and 14. (Black) The fraction of cycles in $\mathbf{C}_n$ with variance greater than $q$.

$\mathbf{C}_n$ are excluded from $\mathbf{C}_n^{1-\gamma}$, the black curve in Figure 5 plots the *total number* of cycles with variance greater than $q$. This shows that a large number of cycles are excluded when we only consider cycles with variance less than about 1.5. The small contribution of cycles with large variance to the sum of degeneracies therefore cannot be attributed to them being fewer in number.

According to these results and the above theorem, virtual processes that are *tightly localised in space* have highly correlated stochastic modulation and make the overwhelmingly dominant contribution to both the ensemble-averaged and individual electron transport at short times. Moreover, in the simulation in Sec. II, we also saw that the loss of this correlation leads to a decay of the electron mobility (also see the supplementary material). These results suggest that *correlated stochastic modulation in the transfer integrals is crucial to charge motion in the STB model*.

## IV. DISCUSSION AND CONCLUSIONS

The results of the analysis in Sec. III show that the STB model can be accurately represented by virtual processes (Feynman diagrams) in which the electron moves through localised regions of the crystal where the stochastic modulation is highly correlated, at least during the first few hundred femtoseconds after excitation of the electron. This time regime includes the early stages of the electron-intermolecular vibrational mode interaction, which occurs on a time scale of at least 100 fs.[1] These results are applicable to both the ensemble-averaged dynamics and the dynamics of individual electrons in the ensemble. We also expected for this result to hold for long time as well; however, we will leave this problem for a future paper. The fact that virtual processes with highly correlated stochastic noise tend to be localised in space may make our results seem trivial. After all, molecular motion far away from where the electron is generated should play a relatively little role in the short time-scale electron dynamics. However, the short time restriction in Eqs. (13) and (14) means that there will be some cutoff $n_0$ for the perturbative expansion in Eq. (7) such that terms with $n > n_0$ can be neglected. Thus, consider two virtual processes containing $n_0$ transitions. Our analysis shows that the virtual process with the higher stochastic noise correlation will make the greater contribution to the electron dynamics on this time scale. The virtual process with the smaller stochastic noise correlation will make the smaller contribution to the electron dynamics, even though it is "accessible" on this time scale (i.e., it is not contained in the neglected part of the perturbative expansion). The key role of virtual processes with correlated stochastic noise at short times therefore appears to be non-trivial. An important point to address is whether it is meaningful to draw conclusions on the electron dynamics using Feynman diagrams and virtual processes. Strictly speaking, virtual processes do not necessarily correspond to the real charge transport physics. On the other hand, Feynman diagrams provide a direct physical model for interpreting the perturbative expansion in Eq. (7).[32] In particular, it would be quite surprising if there was no strong connection between the virtual processes identified here and the actual electron dynamics. An illustrative example can be found in the field of optics, in which a similar approach to the one used in Sec. III is used to interpret the non-linear polarisation.[27,33,34] In this case, Feynman diagrams and virtual processes describe non-linear spectroscopies, which are real experimental phenomena. We are therefore confident that the dominant role of virtual processes with highly correlated stochastic modulation reflects the key role of correlated stochastic motion in charge transport in the STB model.

The connection between "correlated stochastic modulation" and electron transport can be grasped by considering Figure 6. Figure 6 shows a row of molecules erratically rocking about a center of mass. This kind of motion may be significant at room temperature because the molecules are held in the lattice by relatively weak van der Waals forces. As the molecules rock about their center of mass, the relative alignment of the

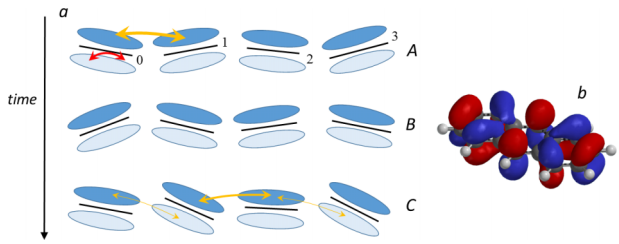


FIG. 6. Diagram to illustrate the relationship between correlated dynamical disorder and electron mobility (see discussion and conclusions). Diagram (a) sketches the time-evolution of a row of planar molecules. The plane of the molecule is drawn as the black line, and the LUMO molecular orbital is drawn as the oval shapes. Here, the stochastic modulation is represented by the molecules rocking erratically about their center of mass (indicated by the red arrow). The two phases of the orbitals are represented by the different shadings. For comparison, the LUMO of anthracene is shown in diagram (b) (calculated with restricted Hartree-Fock with 3-21G* basis in *Spartan* '10 (Ref. 39)). The thickness of the yellow arrows between some of the orbitals indicates how 'bonding' the interaction is.

molecular orbitals change, and the orbital-orbital interactions fluctuate between in-phase "bonding"-type and out-of-phase "antibonding"-type interactions. If the stochastic modulation is highly correlated, then the relative orientations of neighboring orbitals remain stable over a long period of time and a short distance in space. This allows the bonding-type interactions to survive for relatively long lengths of time, allowing charge to shift easily through the crystal. However, if the stochastic modulation has a weak correlation, then the relative orientations of the orbitals of neighboring molecules rapidly fluctuate under the stochastic modulation. Bonding-type orientations of the orbitals can then only survive for a short time and are rapidly changed into "antibonding"-type orientations. This impedes charge transport and restricts charge to a very small region of space. While the cartoon in Figure 6 represents the stochastic modulation in terms of molecules rocking about a center of mass, it must be stressed that the stochastic modulation in the STB model is actually a net outcome of all possible dynamical modes for the crystal lattice. In any case, the interpretation of correlated stochastic modulation and charge transport in terms of relative orientation between molecular orbitals will be valid for any type of mode contributing to the stochastic modulation.

Assuming the applicability of the STB model to real organic crystals, the results of this study suggest that correlation in the dynamical disorder is a key concept necessary for understanding the charge transport mechanism in organic crystals. When the stochastic modulation in the STB model is negligibly small, charge transport is identical to the band picture, with successive orbitals in the crystal interacting to form a delocalised band-type electronic structure. However, with larger stochastic modulation, the relative orientation of successive orbitals must be sufficiently correlated, so that they are correctly aligned to form a band structure that can survive on time scales comparable to charge transport. Correlation cannot survive over large distances, and therefore, only a small number of orbitals in close proximity will ever be aligned properly to form a band (as opposed to an infinite number in the usual band picture). We might then expect for the states of these "bands" to be highly localised. This would explain property (b) mentioned in the introduction. Moreover, we would expect for bonding-type interactions between orbitals in a crystal to survive for shorter lengths of time at higher temperatures because the correlation of the dynamical disorder should decay with temperature. This would cause the "bands" to become increasingly localised, which would explain the loss of charge mobility with temperature seen in real organic crystals, as described by property (a) mentioned in the introduction. This "correlated dynamical disorder-dependent" charge transport mechanism is therefore a self-limiting charge transport mechanism; correlated dynamical disorder is necessary for charge transport but is unable to sustain charge transport for large distances or long times. This mechanism appears to give a qualitative explanation of the unusual charge transport properties of organic crystals; however, it is necessary to build a quantitative charge transport model directly from the concept of correlated fluctuations to confirm this proposal rigorously.

While the concept of "correlated dynamical disorder-dependent" charge transport is understandable physically, some caution is needed when connecting it to the actual temperature dependence of the mobility in real organic crystals. The STB model does not contain temperature explicitly and instead contains two parameters which are both expected to increase with temperature, namely, the decorrelation rate and the amplitude of the stochastic noise. An important point is that our analysis was performed on the basis of a model in which charge transport is dominated by the thermal motions of the molecules in the crystal. This artificial model has a behavior which differs from the anthracene case, namely, that increasing the amplitude of the stochastic modulation leads to an increase in the electron mobility (unless very large stochastic modulation is considered). While we expect our conclusions on the importance of correlated molecular motion to hold for more general cases (see the supplementary material), at this stage, we must restrict ourselves to organic crystals in which the temperature dependence of charge transport is projected mainly through the decorrelation rate parameter rather than the amplitude parameter. This assumption will be true only for certain cases, and it would be an interesting topic for computational and experimental researchers to measure the temperature sensitivity of the decorrelation rate and amplitude of the molecular motion in real organic crystals.

Finally, we make some comments about the model used in this paper. A disadvantage of working with stochastic models is that thermodynamic temperature does not appear directly. In order to connect the decorrelation rate $c$ in our model with the thermodynamic temperature, a separate model in which the Gaussian stochastic modulation is connected with the real phonon dynamics which is necessary. This task is essential for quantitative comparisons between the STB model and experiment; however, it looks very difficult to achieve and is unlikely to build upon the correlation concept developed in this paper. A related problem with stochastic treatments is that dissipation of the electron's energy into the vibrational degrees of freedom of the crystal is neglected. This is probably of little consequence at high temperature;[35,36] however, additional dissipative terms would be needed to apply the model at very low temperatures. Such effects could probably be accounted for by proper incorporation of polaron formation and feedback to the nuclear degrees of freedom. A final issue is that the analysis in Sec. III above was restricted to a one-dimensional lattice; however, two- or three-dimensional lattices would provide more pathways between two points and may change the underlying charge transport dynamics. However, we would still expect that the pathways with highly correlated fluctuations would remain dominant in any case. We are currently working on an algorithmic method for extracting the key virtual processes under more general conditions than presented here, and early results indeed suggest that processes with highly correlated stochastic modulation play the dominant role for more realistic cases in three dimensions. These results will be presented in a future paper.

## ACKNOWLEDGMENTS

This research was supported by grants in aid for Scientific Research KAKENHI (JSPS) No. 26800220 and the World Premier Research Institute Initiative promoted by the Ministry of Education, Culture, Sports, Science, and Tech-

nology of Japan (MEXT) for the Advanced Institute for Materials Research, Tohoku University, Japan. Two anonymous reviewers are thanked for several useful comments.

## APPENDIX: MATHEMATICAL DETAILS OF THE MODEL AND ANALYSIS

### 1. The correlation function

In the correlation function in Eq. (3), the correlation between two neighboring edges was chosen to be half that of the correlation of one edge with itself. A partial justification is as follows. Consider a row of molecules rocking about their center of masses such as in Figure 6 (also see the discussion in the second paragraph of Sec. IV), choose three successive molecules, and label them as 1, 2, and 3, respectively. Suppose that at a particular time, molecules 1 and 2 are oriented such their molecular orbitals are undergoing a low-energy "bonding"-type interaction. By symmetry, we would then expect a probability of about 0.5 that molecule 3 would be oriented in such a way that the molecular orbitals of molecules 2 and 3 are also in a low-energy interaction.

The correlation function in Eq. (3) can be satisfied by setting $X_{uv}(t) = X_u(t) + X_v(t)$ for each edge $uv$, where $X_u(t)$ and $X_v(t)$ are independent Ornstein-Uhlenbeck processes. This method is used in the simulation described in Sec. II. These individual Ornstein-Uhlenbeck processes each follow the equation of motion $\dot{X} = -cX + b\dot{W}$, where $W$ is a Weiner process. The constant $\sigma^2$ in Eq. (3) is equal to the variance of the stationary distribution of these Ornstein-Uhlenbeck processes, which works out to be $\sigma^2 = b^2/2c$.

### 2. Approximation theorem

In this section, we prove the results expressed by Eqs. (12) and (13) of Sec. III. A precise statement of these results is described in the following theorem.

**Theorem.** *For every $n$ greater than some $n_0$, suppose that there exists a $\gamma > 0$ which is independent of $n$ and a subset of $\mathbf{C}_n^{1-\gamma} \subseteq \mathbf{C}_n$ such that*

$$\frac{\sum_{C\in\mathbf{C}_n^{1-\gamma}} \alpha(C)}{\sum_{C\in\mathbf{C}_n} \alpha(C)} > 1-\gamma. \tag{12}$$

*Then we have for arbitrary $k > 0$ and finite $t$,*

(a) $$P_k(t) = P_k^{1-\gamma}(t) + \varepsilon(t), \quad 0 \le |\varepsilon(t)| \le \gamma e^{ct}/(1-\gamma) \tag{13}$$

*providing that $P_k^{1-\gamma}(t)$ is convergent and $\left|P_k^{1-\gamma}(t)\right| \le 1$, where $P_k^{1-\gamma}(t)$ is the cycle expansion in (8) but with the cycles $\mathbf{C}_n$ replaced by the correlated cycles $\mathbf{C}_n^{1-\gamma}$.*

(b) *There is an $n$-independent $\gamma_0 \le \gamma$, superset $\mathbf{C}_n^{1-\gamma_0} \supseteq \mathbf{C}_n^{1-\gamma}$, and a small $\varepsilon$ such that,*

$$\Pr\left(\left|\rho_{kk}(t) - \rho_{kk}^{1-\gamma_0}\right| < \varepsilon e^{ct}\right) = 1 \tag{14}$$

*providing that $\rho_{kk}^{1-\gamma_0}(t)$ is convergent, where $\rho_{kk}^{1-\gamma_0}(t)$ is the perturbative expansion in (7) but calculated only with Feynman diagrams with cycles in $\mathbf{C}_n^{1-\gamma_0}$, and* Pr *is a probability. However, it may be that $\mathbf{C}_n^{1-\gamma_0} = \mathbf{C}_n$ and (14) is satisfied trivially.*

*Proof.* Fix an arbitrary $n$, arbitrary times $\tau_1, \tau_2, \ldots, \tau_n$, and define

$$r_n = a_n^{1-\gamma} + a_n^{\gamma}, \tag{A1}$$

where

$$a_n^{1-\gamma} = \sum_{C\in\mathbf{C}_n^{1-\gamma}} \sum_{f\in\mathbf{F}_+(C)} E\left[f(\tau_1, \ldots, \tau_n)\right] \tag{A2}$$

and

$$a_n^{\gamma} = \sum_{C\in\mathbf{C}_n^{\gamma}} \sum_{f\in\mathbf{F}_+(C)} E\left[f(\tau_1, \ldots, \tau_n)\right], \tag{A3}$$

and the sums in Eqs. (A2) and (A3) run over Feynman diagrams for which the factor $(-1)^h$ in Eq. (9) is positive (the sets $\mathbf{F}_+(C)$). Negative terms will be dealt with separately. We also set $\sigma = 1$ without loss. According to Eq. (9) and the definition of the cycle degeneracy $\alpha(C)$, for each $C$ and any $f \in \mathbf{F}(C)$,

$$E\left[f(\tau_1, \ldots, \tau_n)\right] \ge \alpha(C)\, e^{-ct}. \tag{A4}$$

According to the inequality in (A4) and Eq. (12), we can write

$$\begin{aligned} a_n^{1-\gamma} &\ge \sum_{C\in\mathbf{C}_n^{1-\gamma}} \alpha(C)\, e^{-ct} |\mathbf{F}(C)| \\ &\ge (1-\gamma) D_n e^{-ct} \min_{C\in\mathbf{C}_\gamma^{1-\gamma}} |\mathbf{F}(C)|, \end{aligned} \tag{A5}$$

where $D_n = \sum_{C\in\mathbf{C}_n} \alpha(C)$ is the sum of all degeneracies. Similarly, we have

$$a_n^{\gamma} \le \gamma D_n \max_{C\in\mathbf{C}_n^{\gamma}} |\mathbf{F}(C)|. \tag{A6}$$

Putting these results together gives

$$\frac{a_n^{\gamma}}{a_n^{1-\gamma}} \le \left(\frac{\gamma}{1-\gamma}\right) \frac{e^{ct} \max_{C\in\mathbf{C}_n^{\gamma}} |\mathbf{F}(C)|}{\min_{C\in\mathbf{C}_n^{1-\gamma}} |\mathbf{F}(C)|}. \tag{A7}$$

For any cycle $C$, we have

$$|\mathbf{F}(C)| = \sum_{h=0,2,\ldots,n} \binom{n}{h} \mathbf{1}_{0n}^h(C), \tag{A8}$$

where $\mathbf{1}_{0n}^h(C) = 1$ if the bra makes $h$ transitions in the cycle, begins at 0 and ends at $n$, and $\mathbf{1}_{0n}^h(C) = 0$ otherwise. The factor $n$ chooses $h$ in Eq. (A8), which is the number of ways of ordering the transition times for the bra in the cycle. We can form the trivial bounds,

$$\max_{C\in\mathbf{C}_n^{\gamma}} |\mathbf{F}(C)| \le \sum_{h=0}^{n} \binom{n}{h} = 2^n \tag{A9}$$

and

$$\min_{C\in\mathbf{C}_n^{1-\gamma}} |\mathbf{F}(C)| \ge 1. \tag{A10}$$

These results show that for each $n > n_0$, there is an $\xi_n^{\gamma}$ such that

$$r_n = a_n^{1-\gamma} + \xi_n^{\gamma} a_n^{1-\gamma}, \tag{A11}$$

where

$$\xi_n^{\gamma} \leq \left(\frac{\gamma}{1-\gamma}\right) 2^n e^{ct}. \tag{A12}$$

As for Feynman diagrams in which the factor $(-1)^h$ is negative, we write $s_n = b_n^{1-\gamma} + b_n^{\gamma}$, where $b_n^{1-\gamma}$ and $b_n^{\gamma}$ are defined as in Eqs. (A2) and (A3); however, only Feynman diagrams in which $(-1)^h = -1$ are incorporated into the sums. Proceeding as above, we can obtain

$$-b_n^{1-\gamma} \geq (1-\gamma) D_n e^{-ct} \min_{C \in \mathbf{C}_{\gamma}^{1-\gamma}} |\mathbf{F}(C)| \tag{A13}$$

and

$$-b_n^{\gamma} \leq \gamma D_n \max_{C \in \mathbf{C}_n^{\gamma}} |\mathbf{F}(C)|. \tag{A14}$$

Following steps (A8)–(A10) with appropriate adjustments gives $s_n = b_n^{1-\gamma} + \xi_n^{\gamma} b_n^{1-\gamma}$, with $\xi_n^{\gamma}$ obeying inequality (A12). Substituting $r_n + s_n$ into the cycle expansion (8) and carrying out the integration and summations give

$$P_k(t) = P_k^{1-\gamma}(t) + \varepsilon(t), \tag{A15}$$

where

$$\begin{aligned} |\varepsilon(t)| \leq e^{ct} \left(\frac{\gamma}{1-\gamma}\right) \Bigg| & \sum_{n=2,4,\ldots}^{\infty} (-i/\hbar)^n \\ & \times \sum_{C \in \mathbf{C}_n^{1-\gamma}} \sum_{f \in \mathbf{F}(C)} \int_0^t d\tau_n \int_0^{\tau_n} d\tau_{n-1} \cdots \\ & \times \int_0^{\tau_2} d\tau_1 2^n E[f(\tau_1, \ldots, \tau_n)] \Bigg| \end{aligned} \tag{A16}$$

and $\varepsilon(t) > 0$. However, for each $n$, $2^n E[f(\tau_1, \ldots, \tau_n)]$ is just the correlation function for a Feynman diagram modulated by noise in which the constant $\sigma^2$ in Eq. (3) is replaced with $\left(\sqrt{2}\sigma\right)^2$. So we can rewrite (A16) as

$$|\varepsilon(t)| \leq e^{ct} \left(\frac{\gamma}{1-\gamma}\right) \left|Q_k^{1-\gamma}(t)\right|. \tag{A17}$$

Without loss, we may assume that if $\sigma^2$ is within the range of convergence of $P_k^{1-\gamma}(t)$ (for some given $t$), then so is $\left(\sqrt{2}\sigma\right)^2$ (because we can freely decrease the size of $\sigma^2$ without violating the assumptions of the model). Then we also have that $Q_k^{1-\gamma}(t)$ is well-defined and that $0 \leq \left|Q_k^{1-\gamma}(t)\right| \leq 1$. This completes the proof of (a).

As for part (b), consider a decreasing sequence $\gamma^{(1)}, \gamma^{(2)}, \ldots$ such that $\gamma^{(1)} = \gamma$ and $\gamma^{(r)} \to 0$, and for each $n > n_0$ define the subsets $\mathbf{C}_n^{1-\gamma^{(r)}}$ and $\mathbf{C}_n^{\gamma^{(r)}}$ such that for each $r$, $\mathbf{C}_n^{1-\gamma^{(r)}} \supseteq \mathbf{C}_n^{1-\gamma}$, $\mathbf{C}_n^{\gamma^{(r)}} \subseteq \mathbf{C}_n^{\gamma}$,

$$\sum_{C \in \mathbf{C}_n^{1-\gamma^{(r)}}} \alpha(C) \geq \left(1-\gamma^{(r)}\right) \sum_{C \in \mathbf{C}_n} \alpha(C), \tag{A18}$$

and

$$\sum_{C \in \mathbf{C}_n^{\gamma^{(r)}}} \alpha(C) \leq \gamma^{(r)} \sum_{C \in \mathbf{C}_n} \alpha(C). \tag{A19}$$

We have the limits $\mathbf{C}_n^{1-\gamma^{(r)}} \to \mathbf{C}_n$ and $\mathbf{C}_n^{\gamma^{(r)}} \to \varnothing$ as $r \to \infty$. We extend part (a) to the level of an individual electron in the ensemble by employing the Markov inequality and Borel-Cantelli lemma. By the Markov inequality, we have

$$\begin{aligned} \sum_{r=1}^{\infty} \Pr\left(\left|\rho_{kk}^{1-\gamma^{(r)}} - \rho_{kk}\right| > \eta e^{ct}\right) &= \sum_{r=1}^{\infty} \Pr\left(\left|\rho_{kk}^{\gamma^{(r)}}\right| > \eta\right) \\ &\leq \sum_{r=1}^{\infty} \frac{P_k^{\gamma^{(r)}}(t)}{\eta e^{ct}}, \end{aligned} \tag{A20}$$

for some $\eta > 0$. According to the result in part (a),

$$\sum_{r=1}^{\infty} \frac{P_k^{\gamma^{(r)}}(t)}{\eta e^{ct}} \leq \frac{1}{\eta} \sum_{r=1}^{\infty} \frac{\gamma^{(r)}}{1-\gamma^{(r)}}. \tag{A21}$$

The right-hand side is clearly convergent. By the Borel-Cantelli lemma, we therefore have an $r_0$ such that for $r > r_0$, $\Pr\left(\left|\rho_{kk}^{1-\gamma^{(r)}} - \rho_{kk}\right| < \varepsilon e^{ct}\right) = 1$ for some $\varepsilon$. However, for each $n$, there exists a $k$ such that $\mathbf{C}_n^{\gamma^{(k)}} \neq \varnothing$ and $\mathbf{C}_n^{\gamma^{(j)}} = \varnothing$ for all $j > k$. So it may be that $\mathbf{C}_n^{\gamma^{(r)}} = \varnothing$ and $\rho_{kk}^{1-\gamma^{(r)}} = \rho_{kk}$ for all $r > r_0$ trivially. This proves part (b). □

### 3. Method to generate the cycle space

Let us write, say, the cycle in Figure 2(e) with the notation

$$C = [23,32,21,10,01,12]. \tag{A22}$$

Note that $C$ is an ordered set. The first four elements represent motion of $|0\rangle$ and the final two elements are motion of $\langle 0|$. However, there is no need to explicitly specify whether an element corresponds to $|0\rangle$ or $\langle 0|$, or whether a cycle contains element 0. Consider the cycles $C_1 = [10,01]$, $C_2 = [21,12]$, and $C_3 = [23,32]$. $C_2$ has *positions* at sites 1, 2, and 3, meaning that another cycle can be *embedded* between the left bracket and the left-most edge 21, between edges 21 and 12, and between the right-most edge 12 and the right bracket, respectively. Thus, embedding $C_1$ into position 1 of $C_2$, or into position 2 of $C_2$, or into position 3 of $C_2$ yields

$$A = [[10,01],21,12] = [10,01,21,12], \tag{A23}$$

$$B = [21,[10,01],12] = [21,10,01,12], \tag{A24}$$

and

$$D = [21,12,[10,01]] = [21,12,10,01], \tag{A25}$$

respectively. Of these, only $B$ corresponds to a cycle. This is because only in $B$ are the successive edges adjacent to each other. Thus, the cycle $C$ in (A22) can be obtained by embedding cycle $C_1$ into position 2 of $C_2$, which yields cycle $B$, and then by embedding cycle $C_3$ into position 1 of cycle $B$. Consider a 1D chain $G_N$ of vertices labeled as $-N, -(N-1), \ldots, 0, \ldots, (N-1), N$. The above procedure can be generalized as follows.

**Theorem.** *Any cycle of length n built from the edges of $G_N$ can be obtained by embedding n/2 cycles of length 2 successively into each other.*

*Proof.* Consider a cycle $C'$ of length $n$. In general, $C'$ can be written as

$$C' = [mm', \ldots, m''m]. \tag{A26}$$

Consider walking across the edges in $C'$ in the order $mm', \ldots, m''m$. Suppose that the walk is at vertex $i$ and is about to cross the edge $ij$ for the first time. Then, in order to return to the vertex $m$, the walk must cross the edge $ji$ and return to $i$ a number $h$ steps later. Moreover, $h$ must be even, since $G_N$ is a 1D chain. Thus, there exists two edges $ij$ and $ji$ in $C'$ that are separated by an even number of edges. We can therefore write $C'$ as

$$C' = [mm', \ldots, k'i, [ij, \ldots, ji], ik'' \ldots, m''m], \tag{A27}$$

i.e., as the even-order cycle $[ij, \ldots, ji]$ embedded into the even-order cycle $[mm', \ldots, k'i, ik'' \ldots, m''m]$. Applying this argument iteratively then shows that both $[ij, \ldots, ji]$ and $[mm', \ldots, k'i, ik'' \ldots, m''m]$ can be obtained by starting with a cycle of length 2 and successively embedding other cycles of length 2. □

To generate the cycle spaces $\mathbf{C}_2$, $\mathbf{C}_4$, $\mathbf{C}_6, \ldots, \mathbf{C}_m$ for the chain $G_N$ in the analysis in Sec. III, we first generate the set $\mathbf{C}_2{}'$ from all successive pairs of edges in the chain. We then have that $\mathbf{C}_2{}' = \mathbf{C}_2$. Then, we embed every cycle in $\mathbf{C}_2$ into every position of every cycle in $\mathbf{C}_2$, yielding the set $\mathbf{C}_4{}'$. Following this, we then embed every cycle in $\mathbf{C}_2$ into every position of every cycle in the set $\mathbf{C}_4{}'$, yielding set $\mathbf{C}_6{}'$, and so on. After eliminating any duplicated elements from the sets $\mathbf{C}_4{}'$, $\mathbf{C}_6{}', \ldots$, as well as all elements that do not correspond to real cycles, we find that $\mathbf{C}_l{}' = \mathbf{C}_l$, for $l = 4, 6, \ldots, m$, in accord with the above theorem.


[1]H. Sirringhaus, T. Sukanoue, and J. F. Chang, in *Physics of Organic Semiconductors*, edited by W. Brutting and C. Adachi (Wiley, Germany, 2012).
[2]O. Ostroverkhova, D. G. Cooke, S. Shcherbyna, R. F. Egerton, F. A. Hegmann, R. R. Tykwinski, and J. E. Antony, Phys. Rev. B **71**, 035204 (2005).
[3]N. Karl, Synth. Met. **133**, 649 (2003).
[4]T. Holsein, Ann. Phys. **8**, 343 (1959).
[5]A. S. Eggeman, S. Illig, A. Troisi, H. Sirringhaus, and P. A. Midgley, Nat. Mater. **12**, 1045 (2014).
[6]F. Ortmann, F. Bechstedt, and K. Hannewald, Phys. Status Solidi B **248**, 511 (2011).
[7]F. Ortmann and S. Roche, Phys. Rev. B **84**, 180302 (2011).
[8]Y. Li, V. Coropceanu, and J.-L. Bredas, J. Chem. Phys. **138**, 204713 (2013).
[9]K. Hannewald and P. A. Bobbert, Phys. Rev. B **69**, 075212 (2004).
[10]L. J. Wang, Q. Peng, Q. K. Li, and Z. Shuai, J. Chem. Phys. **127**, 044506 (2007).
[11]D. Wang, L. Chen, R. Zheng, L. Wang, and Q. Shi, J. Chem. Phys. **132**, 081101 (2010).
[12]A. Troisi and G. Orlandi, Phys. Rev. Lett. **96**, 086601 (2006).
[13]H. Tamura, M. Tsukada, H. Ishii, N. Kobayashi, and K. Hirose, Phys. Rev. B **86**, 035208 (2012).
[14]S. Ciuchi and S. Fratini, Phys. Rev. B **86**, 245201 (2012).
[15]L. Wang and D. Beljonne, J. Phys. Chem. Lett. **4**, 1888 (2013).
[16]A. Troisi and G. Orlandi, J. Phys. Chem. A **110**, 4065 (2006).
[17]V. Coropceanu, J. Cornil, D. A. da Silva Filho, Y. Oliver, R. Silbey, and J.-L. Bredas, Chem. Rev. **107**, 926 (2007).
[18]A. Troisi, G. Orlandi, and J. E. Antony, Chem. Mater. **17**, 5024 (2005).
[19]R. Coehoorn and P. A. Bobbert, in *Physics of Organic Semiconductors*, edited by W. Brutting and C. Adachi (Wiley, Germany, 2012).
[20]B. Baumeier, O. Stenzel, C. Poelking, D. Andrienko, and V. Schmidt, Phys. Rev. B **86**, 184202 (2012).
[21]A. Troisi, J. Chem. Phys. **134**, 034702 (2011).
[22]J. L. Doob, Ann. Math. **43**, 351 (1942).
[23]D. T. Gillespie, Phys. Rev. E **54**, 2084 (1996).
[24]J. M. Robertson, V. C. Sinclair, and J. Trotter, Acta Crystallogr. **14**, 697 (1961).
[25]A. N. Aleshin, J. Y. Lee, S. W. Chu, J. S. Kim, and Y. W. Park, Appl. Phys. Lett. **84**, 5383 (2004).
[26]A. A. L. Nicolet, C. Hofman, M. A. Kolchenko, and M. Orrit, Mol. Cryst. Liq. Cryst. **497**, 218 (2008).
[27]P. Hamm and M. Zanni, *Concepts and Methods of 2D Infrared Spectroscopy* (Cambridge, NY, 2011).
[28]L. Isserlis, Biometrika **12**, 134 (1918).
[29]F. W. Wiegel, Phys. Rep. **16**, 57 (1975).
[30]J. Michalowicz, J. M. Nichols, F. Bucholtz, and C. C. Olson, J. Stat. Phys. **136**, 89 (2009).
[31]For (say) the cycle $C = [23, 32, 21, 10, 01, 12]$ (using the notation from the Subsection 3 of the Appendix), the vertex set of $C$ is defined as $\{2, 3, 2, 1, 0, 1, 2\}$. The sum in the cycle variance in Eq. (15) runs over this set.
[32]A. Wuthrich, in *Traditions and Transformations in the History of Quantum Physics*, edited by S. Katzir, C. Lehner, and J. Renn (Max Planck Research Library for the History and Development of Knowledge, Germany, 2010).
[33]S. Mukamel, *Principles of Nonlinear Spectroscopy* (Oxford University Press, NY, 1995).
[34]A. Ishizaki and Y. Tanimura, J. Chem. Phys. **125**, 084501 (2006).
[35]R. Kubo, Adv. Chem. Phys. **15**, 101 (1969).
[36]Y. Tanimura, J. Phys. Soc. Jpn. **75**, 082001 (2006).
[37]G. Csardi and T. Nepusz, InterJournal Complex Systems, 1695 (2006).
[38]*R: A Language and Environment for Statistical Computing* (R Foundation for Statistical Computing, Vienna, Austria, 2012).
[39]Y. Shao *et al.*, Phys. Chem. Chem. Phys. **8**, 3172 (2006).
[40]See supplementary material at http://dx.doi.org/10.1063/1.4916385 for additional simulations of the STB model and discussion of the approach in Sec. III.